Level Set Analysis for Leukocyte Detection and Tracking

Dipti Prasad Mukherjee, *Senior Member, IEEE*, Nilanjan Ray, *Member, IEEE*, and Scott T. Acton, *Senior Member, IEEE*

***Abstract*—We propose a cell detection and tracking solution using image-level sets computed via threshold decomposition. In contrast to existing methods where manual initialization is required to track individual cells, the proposed approach can automatically identify and track multiple cells by exploiting the shape and intensity characteristics of the cells. The capture of the cell boundary is considered as an evolution of a closed curve that maximizes image gradient along the curve enclosing a homogeneous region. An energy functional dependent upon the gradient magnitude along the cell boundary, the region homogeneity within the cell boundary and the spatial overlap of the detected cells is minimized using a variational approach. For tracking between frames, this energy functional is modified considering the spatial and shape consistency of a cell as it moves in the video sequence. The integrated energy functional complements shape-based segmentation with a spatial consistency based tracking technique. We demonstrate that an acceptable, expedient solution of the energy functional is possible through a search of the image-level lines: boundaries of connected components within the level sets obtained by threshold decomposition. The level set analysis can also capture multiple cells in a single frame rather than iteratively computing a single active contour for each individual cell. Results of cell detection using the energy functional approach and the level set approach are presented along with the associated processing time. Results of successful tracking of rolling leukocytes from a number of digital video sequences are reported and compared with the results from a correlation tracking scheme.**

***Index Terms*—Cell detection, level set, tracking.**

I. Introduction

THE OBJECTIVE of this application is to detect and track rolling leukocytes within the microvasculature using video microscopy. Rolling leukocytes are slow-moving (relative to the blood flow) activated white blood cells involved in the inflammatory process. In the focus study used to demonstrate the efficacy of cell identification and tracking, rolling leukocytes are observed *in vivo* using transillumination of living specimens. The study is targeted at the analysis of the inflammatory process and the validation of anti-inflammatory drugs [2], [5]. In order to track a cell and measure the cell velocity and acceleration (two parameters related to the activation level of the cell in the inflammatory process), the first task is to segment the cells from the individual frames of the sequence. Here, we have used image-level set techniques to identify the cells.

Level set analysis from threshold decomposition is a technique that has been utilized in several interesting applications [8], [13]. In the present context, level set analysis provides the advantage of identifying multiple cells in a single frame. Identification of a blood cell is posed as the minimization of an energy functional incorporating image gradient and intensity homogeneity within the closed contour encompassing the cell. The leukocytes in subsequent frames are tracked using the spatial and shape coherency of the cells in the video sequence. Given an identified cell, we attempt to delineate a closed contour in the next frame that minimizes the energy functional quantifying the inter-frame spatial and intensity coherency.

Egmont-Petersen *et al.* have generated synthetic leukocyte images to train a neural network that detects leukocytes in contact with the vessel wall of microvasculature [6]. In our proposed method we have also used the cell geometry information to find the best image-level set that represents a leukocyte. However, our focus is not restricted to leukocytes in contact with the vessel wall, *viz.* with the endothelium. All cells in motion, as opposed to adherent cells, are of interest in our study, since our research team is investigating the mechanism of leukocyte rolling.

Deformable templates are used to segment cells in [7]. The segmentation process proceeds in three sequential steps. In the first step, edges are detected. Next, cell templates are initialized automatically on or near the cells by a Hough transform. Finally, the local deformations of the initialized templates are performed to fine tune the cell segmentation using the detected edges in the first step. In contrast, the method presented here integrates edge detection, cell segmentation, and tracking into a single model.

Sato *et al.* have detected leukocyte motion from the image sequence by observing the image intensities on a spatial path parallel to and near the vessel contour [14]. Their search for cells is limited for the ones that are only rolling along the static vessel contour. They have designed a direction (cells flowing from south-west to north-east) and shape (known width of the leukocyte) sensitive filter and a grouping process that combines thresholded regions of the spatiotemporal image to a cell. The static cell boundary information helps in grouping the cell regions. However, the process is constrained because of the fact that the cells in contact with the vessel wall show spatially restricted motion whereas our approach addresses unrestricted movement of blood cells within the vessel wall.

Wu *et al.* segmented live cell images from the background by first identifying a region that contains a cell using a global threshold [17]. This is followed by localized thresholding within the restricted region containing a cell. It is assumed

Manuscript received May 6, 2002; revised August 14, 2003. The associate editor coordinating the review of this manuscript and approving it for publication was Dr. Nasser Kehtarnavaz.

D. P. Mukherjee is with the Electronics and Communication Sciences Unit, Indian Statistical Institute, Calcutta 700108, India (e-mail: dipti@isical.ac.in).

N. Ray and S. T. Acton are with the Department of Electrical and Computer Engineering, University of Virginia, Charlottesville, VA 22904 USA (e-mail: nray@virginia.edu; acton@virginia.edu).

Digital Object Identifier 10.1109/TIP.2003.819858

that the intensity histogram in this localized region is bimodal. The most vulnerable part of the algorithm in [17] is the use of a single global threshold, which is not robust for intravital (*in vivo*) image analysis, where contrast, focus, and transillumination vary widely. However, individual pixel sensitive local thresholding may be used to extract cell shape given the intra-regional consistency of white blood cells. The area morphology based technique that we have proposed to detect cells (see Section III) uses exhaustive[1] local thresholding implemented through decomposition of image matrix into a stack of binary images. The components representing cells are selected based on cell shape characteristics. The advantage of the use of area morphology over conventional gray-level morphology is that the former does not distort the cell shape dictated by a structuring element used in conventional morphology [1].

In contrast to the morphological or stacking use of the term "level set," level sets are also used in creating a surface that contains a zero-level set representing a curve [15]. In this spirit, geodesic active contours have been used for segmentation and tracking problems [10]. For our intravital video with poor contrast, occlusions, and inconsistent background, segmentation via a single global active contour is insufficient. Often, the rolling leukocytes change contrast from light-on-dark to dark-on-light, and the endothelium (vessel wall) moves due to respiration by the mouse, leading to increased image blur and background motion. Since we are using transillumination to view the venules, other tissue (e.g., muscle) may occlude the venule of interest and may lead to increased image clutter.

Ray *et al.* have used parameterized active contours to track rolling leukocytes [11]. The shape and size sensitive "snakes" improve upon the accuracy provided by traditional centroid and correlation trackers. However, their snake tracker requires time-consuming manual initialization for each individual cell and does not permit automated counting of cells (to measure leukocyte flux, etc.). If the cells were identified first manually, the cell walls could be found using a balloon or "pressure force" snake [4]. Here, we are proposing an integrated technique that combines identification and segmentation. With the snake tracking technique in [11], the computational complexity increases linearly with the numbers of cells tracked. In the proposed method, multiple cells are identified and tracked in a unified approach from a single-level set representation of the entire image frame. We present an integrated energy functional representing image segmentation and tracking and propose a minimization scheme using variational calculus for the energy functional. We show that a satisfactory and computationally attractive solution is tenable by restricting the solution space to the boundaries of connected components in the image-level sets.

In the next section, we present the development of the energy functional to detect a cell. A computationally inexpensive alternative, using level set analysis, is discussed in Section III. The tracking algorithm is developed in Section IV, and results and discussion are presented in Section V, in which a number of digital video sequences are analyzed by the proposed method and a competing approach. Finally, conclusions are given in Section VI.

[1]Exhaustive in the sense that all intensities present in the image are used.

II. Cell Morphology and Detection

In this section, we exploit cell morphology to develop an energy functional that quantifies the solution quality of a given curve that delineates a cell. For the application to leukocytes observed *in vivo*, the segmentation should identify leukocyte-like shapes and ignore nonhomogeneous background fluid (which, in this imagery, is both corpuscular and of plasma). Fig. 1(a) and (b) are two typical leukocyte images—a bright cell and a dark cell. The differing mean intensities are due to defocus, occluding matter (mostly red blood cells) and phase contrast. In each case, the cells contain a homogeneous cytoplasm enveloped by a mostly distinct boundary. The two specific features of the cell intensity profiles include:

1) a typical boundary envelope in which the intensity profile is different from the cell cytoplasm and from the background, if not the entire boundary but at least for a significant part of the border;
2) the leukocyte shapes are nearly circular, except for teardrop-like deformation encountered when in contact with the endothelium [5].

The first step toward extracting leukocyte shape is to find a closed contour that satisfies a leukocyte shape prior and minimizes an energy functional for image segmentation. In the next section, we construct this energy functional.

A. Construction of the Energy Functional

In general, the problem of image segmentation that detects homogeneous region with distinct boundary can be viewed as the placement of a closed curve that maximizes image gradient at its boundary and intensity homogeneity for its interior. Given a parameterized curve $C_i(s) = [X(s), Y(s)]$, $s \in [0,1]$, that separates objects from the background, the energy functional for leukocyte capture should minimize

$$E\left(C_i(s)\right) = -\int_0^1 g\left(|\nabla I|\right) ds - \kappa \int\int_{\wp(C_i)} \mathrm{H}(x,y)dxdy. \quad (1)$$

Here, the first term $\int_0^1 g(|\nabla I|)ds$ integrates image gradient along the curve C_i. The function $g(k)$ is a monotonically increasing function; for example, the classical error function where $g(k) \to 1$ when $k \to \infty$ and $g(0) = 0$. One desirable characteristic of $g(k)$ is that its value should be normalized between [0,1] so that it can be on par with the scale of other terms in the energy functional. A characteristic of the error function is that the value is close to unity beyond certain value of the argument. Thus, a very high gradient magnitude arising out of clutter (such as the strong vessel wall edge) is not given preference over cell edges in the energy functional. Thus, we select $g(k) = (2/\sqrt{\pi}) \int_0^k e^{-t^2} dt$.

In the second term of (1), $\int\int_{\wp(C_i)} \mathrm{H}(x,y)dxdy$ represents the homogeneity of the image region $\wp(C_i)$ bounded by the curve C_i. Region-based strategies for active contour models are discussed extensively in [12]. Here, we relate this homogeneity term to the likelihood of a cell in the following way. Let μ be image intensity within a cell corrupted by additive zero-mean

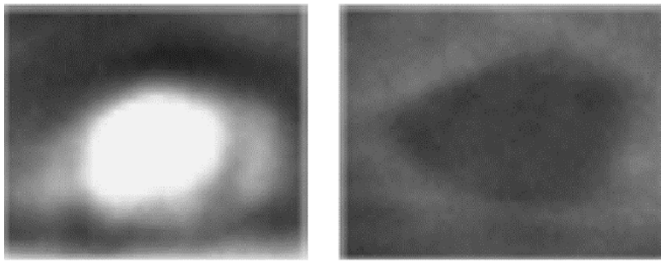

(a) (b)

Fig. 1. (a) Bright leukocyte subimage. (b) Dark leukocyte subimage.

Gaussian i.i.d. noise of variance σ^2. Then the likelihood of the cell given an instance of the contour is as follows:

$$p(I|C_i) \propto \exp\left\{ \sum_{(x,y)\in\wp(C_i)} -\frac{1}{2\sigma^2}\left(I(x,y)-\mu\right)^2 \right\}. \quad (2)$$

Thus, taking the logarithm of (2) and interpreting it in the continuous image domain yields the following definition for $H(x,y)$:

$$H(x,y) = -\frac{\left(I(x,y)-\mu\right)^2}{2\sigma^2}. \quad (3)$$

Similar image-region-based terms have been utilized by Chan and Vese [3] and Yezzi *et al.* [18] for image segmentation. In their approach, image statistics, both inside and outside of the active contour, are considered. In the present case, we only confine our attention to the intensities inside the curve, as the exterior includes the moving background containing clutter.

In the experiments, we estimate μ to be the average intensity within the region, $\wp(C_i)$ $\mu = (\int\int_{\wp(C_i)} I(x,y)dxdy / \int\int_{\wp(C_i)} dxdy)$. This implicit choice of μ is not motivated toward leukocytes appearing dark or bright. Such a choice also eliminates the requirement to determine the parameter value for μ by some explicit means. From (1) and (3), it is evident that σ^2 is absorbed in the weighting parameter κ in (1). The parameter κ in (1) is the weight that controls the relative importance of boundary gradient versus the cytoplasm homogeneity in minimizing E. Following the tracking experiments on training sequences, we set the value of the parameter κ that yields minimum tracking errors (with respect to manual tracking output, i.e., the ground truth). For scenes with significant clutter ($>$ 20 cells per 100 μm venule) and poor contrast, the importance of homogeneity is increased, while for well-contrasted scenes, the gradient magnitude has the higher discriminative power.

In the proposed model, we utilize a speed function for the level set curve that is attracted to the cell cytoplasm. The intensity distribution of the cell cytoplasm is unimodal as approximated using a Gaussian distribution. The level set model introduced in [10] uses a mixture model with either a Gaussian or Laplacian approximation. The difficulty of using such a mixture model analysis in the proposed case is that the background (other than the cell cytoplasm) is not spatially uniform due to the presence of erythrocytes, inactivated leukocytes, and inhomogeneous blood plasma. With a number of training samples from numerous frames at different locations in and around the activated (rolling) white blood cells, we have observed that it is difficult to ascertain a specific mixture distribution model. Also, as the appearance of a deformable white blood cell may change from light-on-dark to dark-on-light due to illumination, the assumption of a global prior probability distribution is not appropriate. Rather, it is more appropriate to search for a homogeneous cell cytoplasm (albeit light or dark).

The energy functional is minimized over different possible configurations of C_i. For the problem of cell detection, we assume that more than one cell cannot partially overlap another. So even though two cells can be mutually osculating, the curves representing leukocytes can neither be intersecting nor circumscribed into one another. Adding this constraint in (1) to guide the evolution of curve C_i, we can write

$$E(C_i) = -\int_0^1 g\left(|\nabla I|\right) ds - \kappa \int\int_{\wp(C_i)} \mathrm{H}(x,y)dxdy + \int\int_{\wp(C_i)} \left(\sum_{j=1, j\neq i}^{N} \chi_j(x,y) \right) dxdy \quad (4)$$

where the function χ_j is the characteristic function for the j^{th} curve representing a leukocyte boundary and is defined as follows:

$$\chi_j(x,y) = \begin{cases} 1, & \text{if } (x,y) \in \wp(C_j) \\ 0, & \text{otherwise} \end{cases} \quad (5)$$

where $\wp(C_j)$ is the region bounded by curve C_j and N is the total number of leukocytes detected in the image. If a pixel (x,y) belongs to multiple curves delineating potential cells, $\Sigma\chi_j$ increases. The summation is minimized in the case that there is no overlap between cell boundaries. Note that the need for the nonoverlapping constraint in the energy functional is crucial, and is comparable to a "hard" constraint. We do not need any additional weight for this component as its value varies linearly with the number of overlapping contours (cells) and with the overlapping area, which is significant compared to the other components of the energy functional.

Then, (4) can be written in the form

$$E(C_i) = -\int_0^1 g\left(|\nabla I|\right) ds - \int\int_{\wp(C_i)} f(x,y)dxdy \quad (6)$$

where

$$f(x,y) = \left(\kappa \mathrm{H}(x,y) - \left(\sum_{j=1, j\neq i}^{N} \chi_j(x,y) \right) \right). \quad (7)$$

Given that leukocytes have a specific range of possible areas and possible deviation from circularity, the energy functional in (6) can be further modified as

$$e(C_i) = \delta\left(\left|\wp(C_i)\right|, \zeta(C_i)\right) E(C_i). \quad (8)$$

Here, we define a delta function $\delta(\cdot)$ that has compact support and has unit value where $a_{\min} \leq \left|\wp(C_i)\right| \leq a_{\max}$ and $c_{\min} \leq \zeta(C_i) \leq c_{\max}$. The circularity measure $\zeta(\cdot)$ is the *slenderness* defined as the ratio of area over perimeter squared.

Since leukocytes are roughly circular in shape and have a specific slenderness measure, this feature is required for recognition in addition to the area constraint. From the known leukocyte shape, the area bound $\{a_{\min}, a_{\max}\}$ and the circularity bound $\{c_{\min}, c_{\max}\}$ are estimated according to established physical models [14].

In the next section we discuss the minimization for the energy functional in (6).

B. Solution of the Energy Functional

The energy functional in (6) is minimized by solving the respective Euler–Lagrange equation as detailed in the Appendix A. The first variation of energy minimization process for (6) is given by

$$\frac{\delta E}{\delta X_i} = -\frac{\partial}{\partial x} g\left(|\nabla I(X_i, Y_i)|\right) - f(X_i, Y_i)\dot{Y}_i \tag{9}$$

$$\frac{\delta E}{\delta Y_i} = -\frac{\partial}{\partial y} g\left(|\nabla I(X_i, Y_i)|\right) + f(X_i, Y_i)\dot{X}_i \tag{10}$$

where the function f is given in (7). Given that $(\dot{Y}_i, -\dot{X}_i) = \mathbf{n}(X_i, Y_i)$ the unit outward normal to the curve at $C_i \equiv (X_i, Y_i)$, the solution for energy minimization is an iterative process where the initial curve is perturbed along local normal direction minimizing the rate of change in energy defined by (9) and (10). A geometric curve evolution equation can be formed using $\Phi_{n+1} = \Phi_n + F|\nabla\Phi|$, where Φ_n is the geometric representation of the curve at n^{th} iteration and F is the speed function [15]. With the solution derived in (9) and (10), the update equation of the curve capturing leukocyte shape is given by

$$\Phi_{n+1} = \Phi_n + t_s\left(-f(x,y)|\nabla\Phi| - \nabla g\left(|\nabla I(x,y)|\right).(\Phi_x, \Phi_y)\right) \tag{11}$$

where t_s is the time step. A similar speed function is also derived in [10]. It can be shown that the curve evolution equation in [10] is a special case of (11) excluding the region homogeneity term and introducing a contour regularity term in the edge gradient part of the energy function in (1).

We are utilizing the gradient descent method to minimize (4). Such a method is known to converge to a local minimum. Note that the energy is bounded given that the intensity range is bounded and the image domain is finite. The discrete implementation of (4), *viz.* (11), is performed with the level set method, which again is known to be a numerically stable iterative process when the Courant–Friedrichs–Levy (CFL) condition involving the time step size t_s is met [15]. In practice, the convergence with such a method is achieved by keeping account of the change in Φ_n in (11) that embeds the evolving level set; although the speed of convergence is dependent on the choice of the time step size t_s in (11).

In Section IV, we demonstrate the extraction of leukocytes through evolution of an initial curve following (11). The drawback of the curve evolution process is the computational expense associated with extracting multiple cells in multiple images. In the next section, we show that an alternate acceptable solution of this proposed minimization is possible through level set morphology.

III. Cell Detection Using Level Set Analysis

To explore a computationally efficient solution space for the energy functional (6), we consider only the boundaries of connected components within the image-level sets that satisfy shape, boundary and region homogeneity constraints detailed in Section II. Before we present this approach, let us explore the properties of the level set decomposition.

A. Level Set Morphology

A complete representation of a digital intensity image is achieved through binary umbrae of the image. A binary umbra is extracted using a threshold decomposition of the image for a particular image intensity level. We refer to this binary umbra containing connected components as an image-level set. Naturally, the binary umbra contains collection of connected components that constitute objects in the image. The boundaries of these connected components are referred to as *level lines*. By analyzing the size and shape of connected components in each level set (i.e., by examining the level set morphology), objects of interest can be extracted.

Let $\Omega \subseteq \Re^2$ be the image domain and $I\colon \Omega \to [0, \Gamma]$, $\Gamma \in \Re$ be an image for which the level set at intensity level $\lambda \in [0, \Gamma]$ is given by

$$I_\lambda = \{(x,y) \in \Omega : I(x,y) \geq \lambda\}. \tag{12}$$

The reconstruction of the original image I is possible through stacking of image-level sets I_λ

$$I(x,y) = \sup\{\lambda : \lambda \in \Gamma, (x,y) \in I_\lambda\}. \tag{13}$$

Therefore, every level set contains connected regions of 1's and 0's where the connectivity is defined in usual 4- or 8-connectivity sense. Henceforth, by connected component we refer to connected regions of 1's.

Fig. 2(a) and (b) is the corresponding level line image for Fig. 1(a) and (b), respectively. For clarity, the level lines are plotted in the intervals of 20 intensity levels in the range of 0–255. Certainly, the leukocyte shape profile is embedded in any one or many of these level lines. Note that by construction, level lines are always closed contours.

We can define area operators on image-level sets [1]. An area-open operator removes connected components of area less than the pre-specified scale from all the level sets of the image. An area-close operator performs identical operation on the complements of the level sets. The sequential concatenation of area open followed by area close for area a is known as *area open-close* operation: $I\hat{\circ}a\hat{\bullet}a$. While area open flattens small bright objects, area close removes small dark objects from the image. As proposed in the next section, we can use the area morphology operations to quickly eliminate components that are not within the possible range of cell sizes.

B. Implementation Using Level Set Analysis

We argue that level set analysis provides an improvement in terms of curve initialization and computational complexity. The entire analysis of (6) assumes a single closed contour. In a given image frame, however, there exist multiple leukocytes that need to be detected. A search process through the level lines

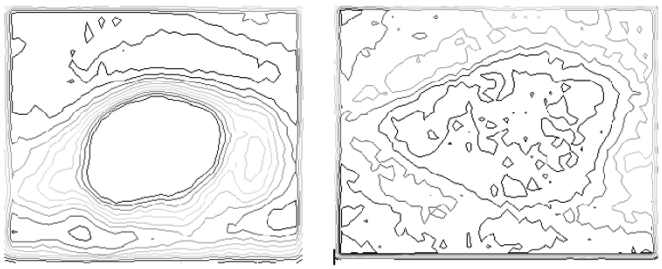

(a) (b)

Fig. 2. (a) Level lines of Fig. 1(a). (b) Level lines of Fig. 1(b).

accommodates simultaneous detection of multiple leukocytes. Note that the contour evolution process of (11) depends on the gradient magnitude maxima, the interior homogeneity and the absence of overlap between multiple contours. The level lines inherently satisfy these properties. By construction, a level line is always a single pixel-thick closed contour and exists for every nonzero image gradient. So, a search for gradient magnitude maxima is equivalent to searching within the level lines. Also, by definition, level lines do not intersect each other. Thus, level lines as leukocyte boundaries satisfy the constraint for nonoverlapping of cells added in (4). Of course, the use of level lines does not preclude actual cell overlap. As explained in previous section, the area open close operator can be used to remove connected components less than a desired size from every level set of the image. In this context, the area open-close operator serves to remove objects with scale less than that of the white blood cells. This also increases internal region homogeneity. By computing the residue of an area open-close operator with a large scale, we can also eliminate objects that are larger than the cell scale.

The start of the minimization process of (6) requires the specification of an initial curve. This initialization is performed manually. The use of level lines, in contrast, precludes any explicit use of initialization as minimization is evaluated for every candidate level line.

Another advantage of using level lines is that the leukocyte shape specific information as specified in (8) can be derived directly from the connected components present in the level sets, thereby pruning the solution space and further reducing the expense. And, since the solution space is bounded by the level sets, the convergence of the minimization process is guaranteed. Furthermore, the exact boundary of the connected component at a particular level set is never distorted, which maintains edge fidelity and localization. Next we describe the actual implementation of this process on a discrete grid.

The algorithm for minimization of the energy functional (4) within the level lines is given by the following.

1) In order to eliminate subscale and above-scale components from I, use area morphology and obtain images $A^{\min}$ and $A^{\max}$:
   a) $A^{\min} = I \hat{\circ} a_{\min} \hat{\bullet} a_{\min}$.
   b) $A^{\max} = I \hat{\circ} a_{\max} \hat{\bullet} a_{\max}$.
2) Define a set of level sets that contains all components of image $A^{\min}$ those are not in $A^{\max}$. That is, $L^{\text{med}}_{\lambda_i} = A^{\min}_{\lambda_i} \oplus A^{\max}_{\lambda_i}$ where level set $L^{\text{med}}_{\lambda_i}$ is derived from image level sets $A^{\min}_{\lambda_i}$ and $A^{\max}_{\lambda_i}$ of images $A^{\min}$ and $A^{\max}$, respectively, at intensity level λ_i.
3) For every level set $L^{\text{med}}_{\lambda_i}$, label connected components $C^{\lambda_i}_j$ from $L^{\text{med}}_{\lambda_i}$ and its complement such that overlapping components from different level sets have the same index j.
4) If $c_{\min} \leq \zeta(C^{\lambda_i}_j) \leq c_{\max}$ evaluate E using (4) for the connected component $C^{\lambda_i}_j$.
5) Assign $E^{\lambda_i}_j$ as the energy value for the leukocyte represented through $C^{\lambda_i}_j$.
6) For each cell index j, find the connected component $C^{\lambda_i}_j$ representing the cell such that $E^{\lambda_i}_j \leq E^{\lambda_k}_j \; \forall \lambda_k \in \Gamma$, $k \neq i$.

Overall, considering only the dominant image processing operations, the level set analysis provides a satisfactory solution in $O(p)$ time where p is the total number of intensity levels present in the image in contrast to the $O(n^2k)$ complexity of the curve evolution (where k is the total number of leukocytes present in the frame and n^2 is the number of pixels in the image). In fact, for the level set analysis approach, there is no need to investigate all the intensity levels present in the image. From the expected intensity features of the cell, a subset of the intensities representing the bright and the dark cells should capture the cell geometry.

However, excessive background clutter and object overlap may require pre-processing of level sets in order to extract the cells. We discuss this process in the next section.

C. Filtering Within Level Sets

It may be necessary to pre-filter the level sets depending on the clutter and in-homogeneity present in the image frame. A typical example of a leukocyte is shown in Fig. 3(a). The corresponding level lines (in the intervals of 20 intensity levels) are shown in Fig. 3(b). Notice that even with the presence of a definite cell, the level lines are connected in such way that the cell region may not meet the area and circularity constraints defined in (8). Therefore, a need exists to reshape the connected components in order to separate the cell boundary from the background. A natural process would be to let the level lines evolve depending on the curvature [15]. The evolution a level line expressed through the zero-level set of a surface Ψ from iteration n to iteration $n+1$ can be expressed as

$$\Psi^{n+1} = \Psi^n + t_s \varsigma \left|\nabla(\Psi^n)\right| \tag{14}$$

where the curvature of the level line is given by ς and time step t_s. The initial Ψ^0 is the signed distance function for a given initial surface typically the image matrix in this case. Fig. 3(c) is an example level line extracted from Fig. 3(b) that contains a leukocyte shape. The evolution of this shape after 200 iterations at the speed proportional to its curvature is shown in Fig. 3(d). Clearly, there is a significant amount of edge distortion, even though a closed, approximately circular contour is obtained.

A computationally attractive alternative to this level line evolution process is possible with minimum shape distortion of level lines. In this case, the level line can be either of convex shape or of concave shape. The question of extraction of leukocytes from the clutter comes only in case of concave shape as

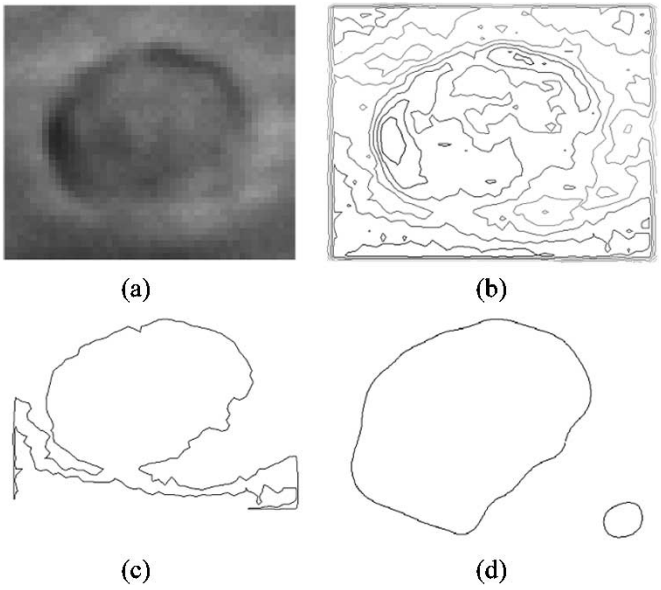

Fig. 3. (a) Original black cell in cluttered background. (b) Level lines of Fig. 3(a). (c) The level line containing potential leukocyte. (d) Level line of Fig. 3(c) after curve evolution.

shown in Fig. 3(c). For a concave shape, the maximum concavity point on the level line is detected from the convex hull of the shape. These points are the maximum distance points on the level line from the bitangent joining concavity entrance points [9].

Refer to Fig. 4(a). For the closed curve P, H is the maximum height point for the concavity bounded by the bitangent EF on the convex hull. The corresponding neck points are H and G having a distance less than the diameter of the leukocyte. The correspondence between neck points is established based on the neck width, the minimum distance between neck points. For a single concavity on the contour, the distance between the neck point and the curve boundary in normal direction is taken as width of the neck. The leukocyte shape can be extracted by splitting adjoining convex boundaries at the neck width. Note in this case that there is no distortion in the level line except for the line representing the neck width.

A formalization of this process is possible using distance transform. Given that the level line is embedded in a two-dimensional (2-D) image matrix, the distance transform of the corresponding level line have minima on the level line and increasing as we move inwards with respect to level line. Note that by construction all the level lines are closed nonintersecting contours. Therefore, a constraint on the distance transform values will shrink the level line. This constraint parameter is the neck width. If a new contour is now drawn with the maximum width limiting to the neck width, concavities can be split into convex shapes.

Let L be the level set in which we want to isolate the leukocyte from clutter. Let D denote the distance transform of the complement of L as follows:

$$D = \text{dist}(\sim L). \tag{15}$$

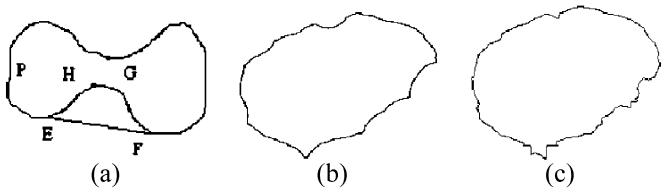

Fig. 4. (a) For the closed contour P, points E and F are concavity entrance points on the convex hull of P and H is the concavity height point at maximum distance from EF. Corresponding to two concavities H and G are two neck points. (b) Level line of Fig. 3(c) after constraining distance transform space by the amount of the neck width. (c) The re-grown contour of Fig. 4(b).

If l is the distance between corresponding pair of neck points, we generate the eroded-level set image M as follows:

$$M(x,y) = \begin{cases} 1, & \text{if } D(x,y) > \frac{l}{2} \\ 0, & \text{else.} \end{cases} \tag{16}$$

Note that M also has a closed contour that is disconnected from the rest of the level line at the neck points. The eroded-level line can be re-grown using dilation by the same $l/2$ distance. For the level line in Fig. 3(c), the modified contour after constraining the distance transform according to the neck width is shown in Fig. 4(b). The corresponding dilated level line is shown in Fig. 4(c).

Given a set of curves in an image corresponding to potential cell boundaries, we can address the correspondence of the set of curves with corresponding curves in subsequent frames. In the next section, we present the tracking technique that establishes the correspondence between identified leukocyte contours in consecutive frames.

IV. Tracking

The problem of leukocyte tracking in multiple image frames can be cast as the problem of maximizing a similarity measure between level sets in consecutive frames. Given the search space used in Section III, the process of establishing correspondence is now reduced between selected connected components representing potential leukocytes.

We can attack the tracking problem as the detection of a closed-level line in the n^{th} frame given the best description of leukocyte boundary in $(n-1)^{\text{th}}$ frame. Therefore, in the current frame, we would like to minimize the energy associated with leukocyte boundary detection as suggested by (6) and then match that boundary with that of the previous frame. Then the energy functional for quantifying the solution quality of tracking is

$$E(C_i) = \frac{1}{2}(E_{\text{cur}} - E_{\text{prev}})^2 + E_{\text{cons}} \tag{17}$$

where

$$E_{\text{cur}} = -\int_0^1 g\left(|\nabla I|\right) ds - \kappa \int\int_{\wp(C_i)} H(x,y)dxdy \tag{18}$$

and E_{cons} can be taken as the difference of cell centroid position $(\overline{x}_{\text{cur}}, \overline{y}_{\text{cur}})$ in the current frame and that in the previous frame $(\overline{x}_{\text{prev}}, \overline{y}_{\text{prev}})$ plus the overlap minimizing term for multiple cell tracking: $E_{\text{cons}} = ||(\overline{x}_{\text{cur}}, \overline{y}_{\text{cur}}) -$

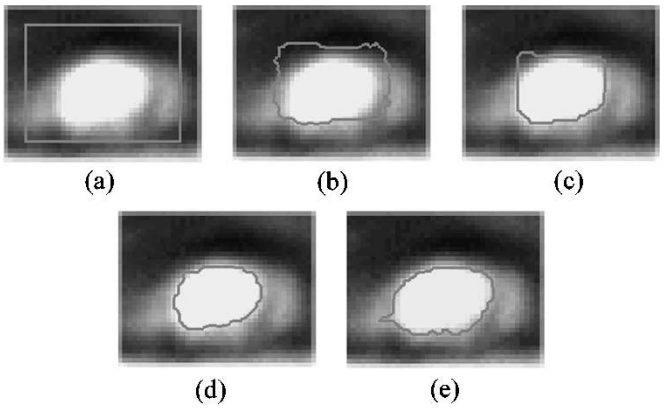

Fig. 5. (a) The initial curve on the bright cell image of Fig. 1(a). The curve is evolved following solution of the objective function (6) in Section II-B. (b) After 1000 iterations. (c) After 2000 iterations. (d) After 3200 iterations. (e) Using area morphology-based level set analysis method.

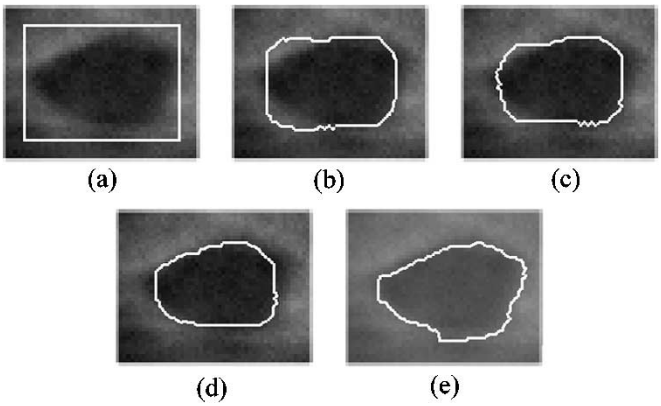

Fig. 6. (a) The initial level curve on the dark cell image of Fig. 1(b) that is evolved as per derivation in Section II-B. (b) After 1000 iterations. (c) After 2000 iterations. (d) After 2700 iterations. (e) Using level set analysis method.

$(\overline{x}_{\rm prev}, \overline{y}_{\rm prev})||^2 + \int\int_{\wp(C_i)} (\sum_{j=1, j\neq 1}^{N} \chi_j(x,y))dxdy$. The gradient magnitude and homogeneity energy evaluated at the current frame is $E_{\rm cur}$ while that of the previous frame is $E_{\rm prev}$. Minimization of their difference in (17) ensures shape consistency of the leukocyte as one move along frame. To maintain spatial coherency in video frames captured typically at 25 fps, it is reasonable to assume that between frames cell movements are marginal. For a fast rolling cell at 30 μm/s, the cell moves only 3 pixels per frame using 320 $\times$ 240 images at 30 fps. While tracking multiple cells, the correspondences between cells are established through evaluation of minimum spatial distance between cell centroids in consecutive frames. Since, the centroid coordinates can be expressed as the ratio of moments about the x- and y-axis with respect to the area of the shape respectively, then $E_{\rm cons}$ is given by

$$E_{\rm cons} = \int\int_{\wp(C_i)} \left(\sum_{j=1, j\neq i}^{N} \chi_j(x,y) \right) dxdy + \frac{1}{2A} \left(\int\int_{\wp(C_i)} (x - \bar{x}_{\rm prev}) dxdy \right)^2 + \frac{1}{2A} \left(\int\int_{\wp(C_i)} (y - \bar{y}_{\rm prev}) dxdy \right)^2 \quad (19)$$

where A is the area of the evolved curve. Following derivation in Appendix B, the curve update equation in line with the development in (11) is given by

$$\Phi_{n+1} = \Phi_n + t_s \left((E_{\rm cur} - E_{\rm prev}) \left(-\kappa H(x,y) |\nabla \Phi| - \nabla g \left(|\nabla I(x,y)| \right) . (\Phi_x, \Phi_y) \right) + q(x,y) |\nabla \Phi| \right) \quad (20)$$

where t_s is the time step.

In the next section, we show the result of cell detection and tracking on a number video sequences and compare them with established approaches.

V. Results and Discussion

The video sequences are recorded via transillumination of the mouse cremaster at 25 fps frame rate using a Pixelfly digital camera. The frame resolution is 640 $\times$ 480 pixels where the pixel to micron ratio is 4.94 pixels/μm in the horizontal direction and 4.68 pixels/μm in the vertical direction. In the present implementation of the software, the user specifies a region for segmentation and subsequent tracking. Note that the region typically contains multiple cells. The tracking result with the trajectories of each cells as the tracking progresses are shown in an accompanying window.

We begin with the extraction of typical leukocyte shapes shown in Fig. 1(a) and (b), respectively. Fig. 5(a)–(d) shows the progression of an initial curve toward the shape of the bright blood cell. The initial curve is modified as per the solution (11) of the energy functional (6). The initialization is done with a rectangular curve as shown in Fig. 5(a), and Fig. 5(b), (c), and (d) are the positions of the initial curve after 1000, 2000, and 3200 iterations, respectively. For implementation in the digital space, a curvature smoothness term is added to the solution. The corresponding processing times in MATLAB implementation are 5.1, 10.4, and 16.8 s for Fig. 5(b), (c), and (d), respectively. The leukocyte shape extraction using area morphology-based level set method is shown in Fig. 5(e) and the corresponding processing time is 1.06 s. Clearly, a reasonably good shape extraction is achieved with the level set searching process in a computationally inexpensive way.

The identical result is obtained for the dark cell in Fig. 1(b). The evolution of an initial closed curve as per the solution of the energy functional (6) developed in Section II-B is shown in Fig. 6(a)–(d). While Fig. 6(a) is the initial curve, Fig. 6(b), (c), and (d) show the curve evolution after 1000, 2000, and 2700 iterations with the processing times of 6.9, 13.85, and 19.11 s, respectively. The result obtained using level set method, shown in Fig. 6(e), has captured the dark cell in only 1.2 s.

The result of level set curve-evolution process using only edge gradient term and without utilizing the region homogeneity terms of (1) on identical cells of Fig. 5(a) and (6a) are shown in Figs. 7(a) and (b), respectively. In both cases, even after 2500 iterations, the cell morphology cannot be extracted.

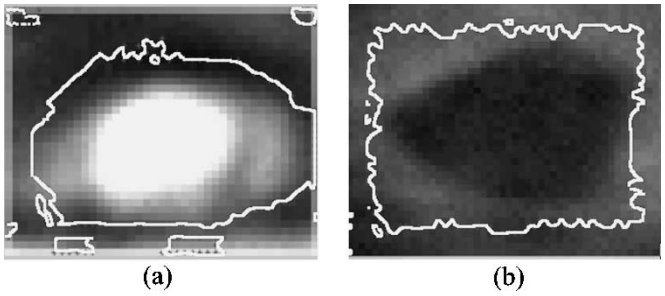

Fig. 7. Level set curve evolution after 2500 iterations without using the region homogeneity term for (a) the bright and (b) the dark cells.

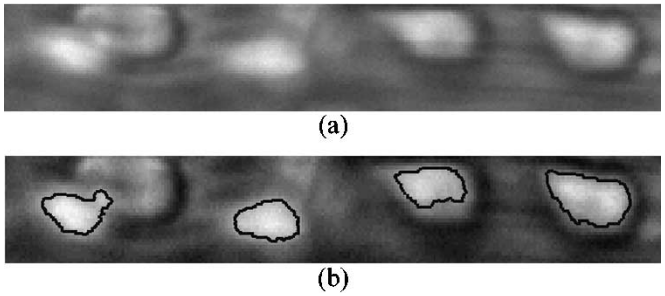

Fig. 8. (a) Original image containing four cells. (b) Contour extracted using the level set approach.

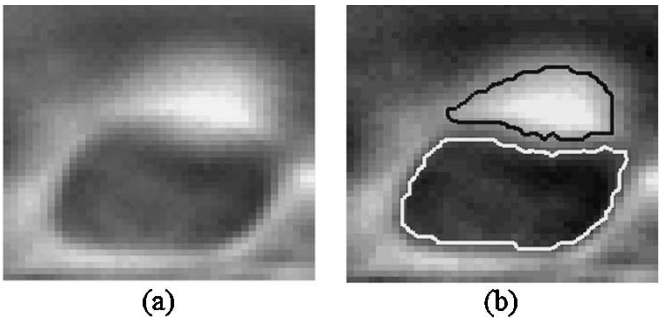

Fig. 9. (a) Original image containing one bright cell and a dark cell where the bright cell is partially occluded by the dark cell. (b) Contour extracted using the level set approach.

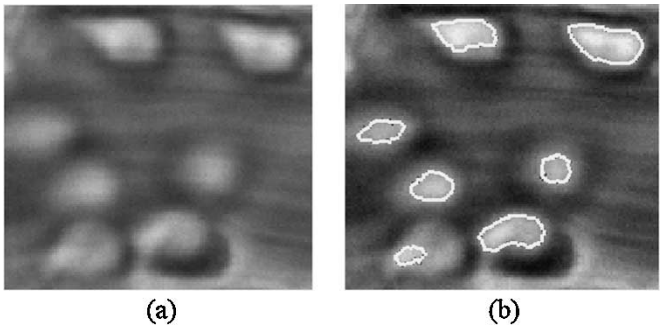

Fig. 10. (a) Original image containing multiple cells. (b) Contour extracted using the level set approach.

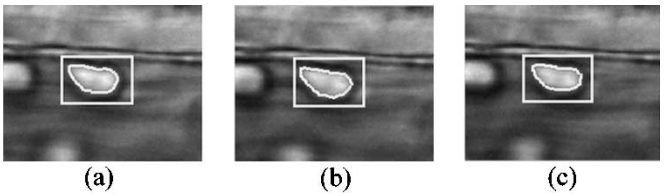

Fig. 11. (a)–(c): Tracking result for the first, fifth, and tenth frames, respectively. In each case, initialization is done using the rectangular zero-level set function.

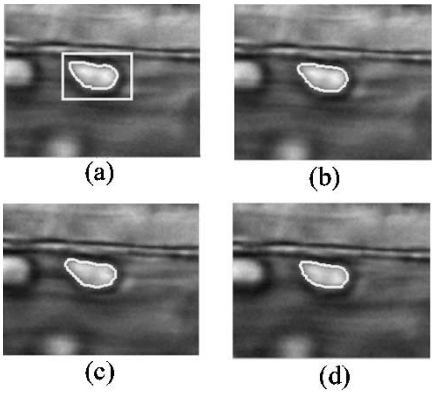

Fig. 12. (a) Identical initialization as in Fig. 11(a). (b) The zero-level set captures the cell shape after 90 iterations. (c), (d) The zero-level sets of (b) and (c) are deformed to capture the shape in the fifth and tenth frame, respectively.

Next, we investigate the accuracy of segmentation in case of multiple cells. Fig. 8(a) is an image containing four white cells. The segmented image using the level set approach is shown in Fig. 8(b). In the second image in Fig. 9(a), where a dark cell is almost occluding a bright cell, the level set approach could separate the cells with closed contours despite their proximity, as shown in Fig. 9(b). Note that our approach is successful in extracting the shape even though the dark cell cytoplasm is connected to the inhomogeneous background.

The third image of Fig. 10(a) contains multiple leukocytes. The segmented result is shown in Fig. 10(b). We can see that all but one dark cell is extracted through the segmentation process.

Overall, as the level lines are inherently guaranteed to be single-pixel thick closed contours, the analysis of cell morphology is easily facilitated. For example, the area, centroid, and orientation of a cell can easily be evaluated from level lines that do not require post-processing such as edge thinning and linking, as do detected edges.

A representative tracking result using the level set approach is presented for a ten-frame sequence. In the first case, the cell under consideration is segmented in each frame separately with initialization using rectangular zero-level set function. So, no additional tracking related constraints are added to segment the cell. The result of such segmentation is shown in Fig. 11(a)–(c). For segmentation, the corresponding contour iterations are 110, 80, and 80 for the first, second, and third frames shown, respectively. In Fig. 12, the same sequence is initialized in the first frame similar to Fig. 11(a). The initialization for the entire sequence is shown in Fig. 12(a). Fig. 12(b) shows the correct extraction of cell shape for the first frame after 110 iterations. Fig. 12(c) and (d) is successful cell detection for the fifth and tenth frame after deforming the zero-level set of Fig. 12(b) and (c) after 90 and 80 iterations, respectively.

Tracking results are provided in comparison with a standard correlation tracker. Note that the correlation tracker requires manual initialization within the first frame. This initialization

TABLE I
AVERAGE NUMBER OF FRAMES TRACKED FOR FOUR TEST SEQUENCES

Method	% Frames tracked			
	Sequence 1	Sequence 2	Sequence 3	Sequence 4
Level set	88	85	91	96
Correlation	71	68	81	72

TABLE II
RMSE FOR NUMBER OF FRAME TRACKED FOR FOUR TEST SEQUENCES

Method	RMSE			
	Sequence 1	Sequence 2	Sequence 3	Sequence 4
Level set	6.2	4.9	7.5	3.2
Correlation	9.6	14.9	13.1	8.3

process identifies the leukocyte center in the first frame and creates a template of the leukocyte. In the second frame, a search window is identified and the normalized cross-correlation is maximized to locate the cell position. The same procedure is repeated for subsequent frames. For more information on the use of correlation trackers for tracking leukocytes *in vivo*, see [2].

In contrast to the correlation tracker, the proposed level set tracker is automatic and does not require initialization. The proposed level set tracker is not affected by slight deformations or rotations of the leukocyte observed within an intravital video sequence. While the correlation tracker performs template matching separately for individual leukocytes, the tracking via level set segmentation occurs simultaneously and uniformly for all leukocytes. We utilize the following two measures to compare the results.

1) Average number of frames successfully tracked in each sequence is calculated. For each cell, the number of frames tracked is recorded and these results are averaged using number of cells tracked in each frame. A frame is considered as successfully tracked if the measured cell center is within one cell radius of the manually recorded cell center.
2) The root mean square errors (rmse) of the cell center positions in tracked frames are estimated with respect to the ground truth provided by human.

In this paper, we report the results from four digital sequences. The results for the average number of frame tracked are given in the Table I while the rmse of the cell center position with respect to ground truth is shown in Table II. In each case, we have tracked 25 frames and the rmse is averaged over 25 frames. In both counts, level set tracker performance is better than the correlation tracker without even requiring any expert initialization.

VI. CONCLUSIONS

The proposed technique utilizes image-level lines to capture multiple rolling leukocytes. In contrast to level set functions where an initialized level curve is evolved for image segmentation that is sensitive to local image gradient and noise, a set of level lines is efficiently examined in terms of shape, size, internal homogeneity, and overlap with other segments. Cell tracking is implemented through spatial consistency and intensity coherency among the detected cells in the consecutive frames. A major contribution is the construction of a unified energy function to integrate segmentation and tracking. An acceptable and computationally attractive solution is introduced using image-level set analysis. The results show considerable improvement over the existing correlation tracker. A major advantage for the proposed tracker is that it does not require any manual initialization, as opposed to the existing cell tracking systems.

APPENDIX A

Selecting $E_1 = \int_0^1 g(|\nabla I|)ds = \int_0^1 T(X,Y)ds$, the corresponding Euler equations are obtained from the first variation of the energy functional [16]

$$\frac{\delta E_1}{\delta X} = \frac{\partial}{\partial X}T(X,Y) = \frac{\partial T}{\partial x}$$
$$\frac{\delta E_1}{\delta Y} = \frac{\partial}{\partial Y}T(X,Y) = \frac{\partial T}{\partial y}. \tag{A.1}$$

The computational complexity of evaluating the region integral for the energy component E_2 can be minimized applying Green's theorem and converting the region integral into a line integral. The region integral for $f(x,y)$ in (6) can be written as

$$E_2 = \int\int_{\wp(C_i(s))} f(x,y)dxdy = \int\int_{\wp(C_i(s))} \left(\frac{\partial Q}{\partial x} - \frac{\partial P}{\partial y}\right)dxdy$$
$$= \int_0^1 \left(P\frac{dX}{ds} + Q\frac{dY}{ds}\right)ds \tag{A.2}$$

where P and Q are $P = -(1/2)\int_0^Y f(X,t)dt$ and $Q = (1/2)\int_0^X f(t,Y)dt$, respectively, such that $f(X,Y) = (\partial Q/\partial X) - (\partial P/\partial Y)$. Therefore, the energy component E_2 can be expressed as $E_2 = \int_0^1 G(s,X,Y,\dot{X},\dot{Y})ds$, where $G(s,X,Y,\dot{X},\dot{Y}) = P\dot{X} + Q\dot{Y}$ with $\dot{X} = (dX/ds)$, $\dot{Y} = (dY/ds)$. Again applying the variational principle, the following Euler equations are derived by equating the first variation to zero:

$$\frac{\delta E_2}{\delta X} = \frac{\partial G}{\partial X} - \frac{d}{ds}\left(\frac{\partial G}{\partial \dot{X}}\right) = 0$$
$$\frac{\delta E_2}{\delta Y} = \frac{\partial G}{\partial Y} - \frac{d}{ds}\left(\frac{\partial G}{\partial \dot{Y}}\right) = 0. \tag{A.3}$$

The solution of (A.3) can be further reduced as

$$\frac{\delta E_2}{\delta X} = \frac{\partial G}{\partial X} - \frac{d}{ds}\left(\frac{\partial G}{\partial \dot{X}}\right) = \frac{\partial P}{\partial X}\dot{X} + \frac{\partial Q}{\partial X}\dot{Y} - \frac{dP}{ds}$$
$$= \frac{\partial P}{\partial X}\dot{X} + \frac{\partial Q}{\partial X}\dot{Y} - \frac{\partial P}{\partial X}\dot{X} - \frac{\partial P}{\partial Y}\dot{Y}$$
$$= \left(\frac{\partial Q}{\partial X} - \frac{\partial P}{\partial Y}\right)\dot{Y} = f(X,Y)\dot{Y}. \tag{A.4}$$

Similarly, we have

$$\begin{aligned}\frac{\delta E_2}{\delta Y} &= \frac{\partial G}{\partial Y} - \frac{d}{ds}\left(\frac{\partial G}{\partial \dot{Y}}\right) = \frac{\partial P}{\partial Y}\dot{X} + \frac{\partial Q}{\partial Y}\dot{Y} - \frac{dQ}{ds} \\ &= \frac{\partial P}{\partial Y}\dot{X} + \frac{\partial Q}{\partial Y}\dot{Y} - \frac{\partial Q}{\partial X}\dot{X} - \frac{\partial Q}{\partial Y}\dot{Y} \\ &= -\left(\frac{\partial Q}{\partial X} - \frac{\partial P}{\partial Y}\right)\dot{X} = -f(X,Y)\dot{X}. \qquad \text{(A.5)}\end{aligned}$$

Therefore, combining the terms for energy E_1 and E_2 from (A.1), (A.4) and (A.5), the first variation of energy minimization process for (6) is given by

$$\begin{aligned}\frac{\delta E}{\delta X} &= -\frac{\partial}{\partial x} g\left(|\nabla I(X,Y)|\right) - f(X,Y)\dot{Y} \\ \frac{\delta E}{\delta Y} &= -\frac{\partial}{\partial y} g\left(|\nabla I(X,Y)|\right) + f(X,Y)\dot{X} \qquad \text{(A.6)}\end{aligned}$$

where the function f is given in (7).

APPENDIX B

Applying the variational principle to (17) we obtain the first variation as follows:

$$\begin{aligned}\frac{\delta E}{\delta X} &= (E_{\text{cur}} - E_{\text{prev}})\frac{\delta E_{\text{cur}}}{\delta X} + \frac{\delta E_{\text{cons}}}{\delta X}, \text{ and} \\ \frac{\delta E}{\delta Y} &= (E_{\text{cur}} - E_{\text{prev}})\frac{\delta E_{\text{cur}}}{\delta Y} + \frac{\delta E_{\text{cons}}}{\delta Y}. \qquad \text{(B.1)}\end{aligned}$$

Using derivations in the Appendix A, we can rewrite (B.1) as follows:

$$\begin{aligned}\frac{\delta}{\delta X} E_{\text{cur}} &= -\frac{\partial}{\partial x} g\left(|\nabla I(X,Y)|\right) - \kappa H(X,Y)\dot{Y} \\ \frac{\delta}{\delta Y} E_{\text{cur}} &= -\frac{\partial}{\partial y} g\left(|\nabla I(X,Y)|\right) + \kappa H(X,Y)\dot{X}. \qquad \text{(B.2)}\end{aligned}$$

Applying the same technique to (19), we obtain

$$\begin{aligned}\frac{\delta}{\delta X} E_{\text{cons}} = \Bigg[&\left(\sum_{j=1, j\neq i}^{N} \chi_j(X,Y)\right) \\ &+ \frac{1}{A}\left(\iint_{\wp(C_i)} (x - \bar{x}_{\text{prev}})dxdy\right)(X - \bar{x}_{\text{prev}}) \\ &+ \frac{1}{A}\left(\iint_{\wp(C_i)} (y - \bar{y}_{\text{prev}})dxdy\right)(Y - \bar{y}_{\text{prev}})\Bigg]\dot{Y}\end{aligned}$$

and

$$\begin{aligned}\frac{\delta}{\delta Y} E_{\text{cons}} = -\Bigg[&\left(\sum_{j=1, j\neq i}^{N} \chi_j(X,Y)\right) \\ &+ \frac{1}{A}\left(\iint_{\wp(C_i)} (x - \bar{x}_{\text{prev}})dxdy\right)(X - \bar{x}_{\text{prev}}) \\ &+ \frac{1}{A}\left(\iint_{\wp(C_i)} (y - \bar{y}_{\text{prev}})dxdy\right) \\ &\times (Y - \bar{y}_{\text{prev}})\Bigg]\dot{X}. \qquad \text{(B.3)}\end{aligned}$$

So, combining (B.1) and (B.3), we find the following Euler equation:

$$\begin{aligned}&(E_{\text{cur}} - E_{\text{prev}})\left(-\nabla g\left(|\nabla I(X,Y)|\right)\right. \\ &\quad \left. -\kappa H(X,Y)\mathbf{n}(X,Y)\right) + q(X,Y)\mathbf{n}(X,Y) = 0, \qquad \text{(B.4)}\end{aligned}$$

where $q(x,y)$ is defined as

$$\begin{aligned}q(X,Y) = &\sum_{j=1, j\neq i}^{N} \chi_j(X,Y) + \frac{1}{A}\left(\iint_{\wp(C_i)} (x - \bar{x}_{\text{prev}})dxdy\right) \\ &\times (X - \bar{x}_{\text{prev}}) + \frac{1}{A}\left(\iint_{\wp(C_i)} (y - \bar{y}_{\text{prev}})dxdy\right)(Y - \bar{y}_{\text{prev}}) \qquad \text{(B.5)}\end{aligned}$$

REFERENCES

[1] S. T. Acton and D. P. Mukherjee, "Scale space classification using area morphology," *IEEE Trans. Image Processing*, vol. 9, pp. 623–635, Apr. 2000.

[2] S. T. Acton, K. Wethmar, and K. Ley, "Automatic tracking of rolling leukocytes in vivo," *Microvasc. Res.*, vol. 63, pp. 139–148, 2002.

[3] T. F. Chan and L. A. Vese, "Active contours without edges," *IEEE Trans. Image Processing*, vol. 10, pp. 266–277, Feb. 2001.

[4] L. D. Cohen and I. Cohen, "Finite element methods for active contour models and balloons for 2-D and 3-D images," *IEEE Trans. Pattern Anal. Machine Intell.*, vol. 15, pp. 1131–1147, Nov. 1993.

[5] E. R. Damiano, J. Westheider, A. Tözeren, and K. Ley, "Variation in the velocity, deformation, and adhesion energy density of leukocytes rolling within venules," *Circ. Res.*, vol. 79, pp. 1122–1130, 1996.

[6] M. Egmont-Petersen, S. C. Tromp, T. M. Lehmann, D. W. Slaaf, and T. Arts, "Detection of leukocytes in contact with the vessel wall from in vivo microscope recordings using a neural network," *IEEE Trans. Biomed. Eng.*, vol. 47, pp. 941–951, July 2000.

[7] A. Garrido and N. Perez de la Blanca, "Applying deformable templates for cell image segmentation," *Pattern Recognit.*, vol. 33, pp. 821–832, 2000.

[8] D. P. Mukherjee and S. T. Acton, "Cloud tracking using scale space classification," *IEEE Trans. Geosci. Remote Sensing*, vol. 40, pp. 405–415, Feb. 2002.

[9] D. P. Mukherjee, A. Zisserman, and M. Brady, "Shape from symmetry—detecting and exploiting symmetry in affine images," *Philosoph. Trans. Roy. Soc. London*, ser. A, vol. 351, pp. 77–106, 1995.

[10] N. Paragios and R. Deriche, "Geodesic active contours and level sets for the detection and tracking of moving objects," *IEEE Trans. Pattern Anal. Machine Intell.*, vol. 22, pp. 266–280, Mar. 2000.

[11] N. Ray, S. T. Acton, and K. Ley, "Tracking leukocytes in vivo with shape and size constrained active contours," *IEEE Trans. Med. Imaging*, vol. 21, pp. 1222–1235, Oct. 2002.

[12] R. Ronfard, "Region-based strategies for active contour models," *Int. J. Comput. Vis.*, vol. 13, pp. 229–251, 1994.

[13] P. Salembier and J. Serra, "Flat zones filtering, connected operators and filters by reconstruction," *IEEE Trans. Image Processing*, vol. 4, pp. 1153–1160, Aug. 1995.

[14] Y. Sato, J. Chen, R. A. Zoroofi, N. Harada, S. Tamura, and T. Shiga, "Automatic extraction and measurement of leukocyte motion in microvessels using spatiotemporal image analysis," *IEEE Trans. Biomed. Eng.*, vol. 44, pp. 225–236, Apr. 1997.

[15] J. A. Sethian, *Level Set Methods and Fast Marching Methods*. Cambridge, U.K.: Cambridge Univ. Press, 1999.

[16] J. L. Troutman, *Variational Calculus With Elementary Convexity*. New York: Springer-Verlag, 1983.

[17] K. Wu, D. Gauthier, and M. D. Levine, "Live cell image segmentation," *IEEE Trans. Biomed. Eng.*, vol. 42, pp. 1–12, Jan. 1995.

[18] A. Yezzi, A. Tsai, and A. Willsky, "A statistical approach to snakes for bimodal and trimodal imagery," in *Proc. 7th IEEE Int. Conf. Computer Vision*, Corfu, Greece, Oct. 1999.

Dipti Prasad Mukherjee (M'01–SM'04) received the B.E. degree from Jadavpur University, India, in 1985, the M.S. degree from the University of Saskatchewan, Canada, in 1989, and the Ph.D. degree from the Indian Statistical Institute (ISI), Calcutta, in 1996.

He is currently an Associate Professor with the Electronics and Communication Sciences Unit, ISI. He was a Visiting Assistant Professor at Oklahoma State University, Stillwater, in 1998-1999 and a Research Scientist in the Electrical and Computer Engineering Department, University of Virginia, Charlottesville, in 2002. He was a UNDP Fellow with the Robotics Research Group, University of Oxford, U.K., in 1992. His research interests are in the areas of computer vision and graphics. He has published more than 25 peer-reviewed journal papers and is the author of a text book on computer graphics and multimedia and an edited book on pattern recognition.

Dr. Mukherjee was the recipient of UNESCO-CIMPA fellowships to INRIA, France, in 1991, 1993, and 1995 and fellowships to ICTP, Trieste, Italy in 2000.

Nilanjan Ray (S'03) received the B.S. degree in mechanical engineering from Jadavpur University, Calcutta, India, in 1995, the M.Tech. degree in computer science from the Indian Statistical Institute, Calcutta, in 1997, and the Ph.D. degree in electrical engineering from the University of Virginia, Charlottesville, in 2003.

Currently, he is a postdoctoral Research Associate with the Electrical and Computer Engineering Department, University of Virginia. His research interests include active contour models, object tracking using Monte Carlo methods, applications of partial differential equations in image processing, and connected filtering.

Dr. Ray is a recipient of the CIMPA-UNESCO fellowship for image processing in 1999 and a graduate fellowship at the Indian Statistical Institute from 1995 to 1997. He also received the Best Student Paper Award at the IEEE International Conference on Image Processing in 2002 from the IBM Picture Processing Society.

Scott T. Acton (S'83–M'93–SM'99) received the B.S. degree in electrical engineering from Virginia Tech, Blacksburg, in 1988 and the M.S. and Ph.D. degrees in electrical and computer engineering from the University of Texas at Austin in 1990 and 1993, respectively.

He holds appointments in both electrical and computer engineering and biomedical engineering at the University of Virginia, Charlottesville. He was named the Outstanding New Teacher in 2002, elected a Faculty Fellow in 2003, and is the Walter N. Munster Chair for Intelligence Enhancement. He has worked in industry for AT&T, the MITRE Corporation, and Motorola, Inc., and in academia for Oklahoma State University. His research interests include biomedical image analysis, multiscale signal representations, diffusion algorithms, active contours, video tracking, image morphology, image segmentation, and content-based image retrieval.

Dr. Acton has served as Associate Editor for the IEEE TRANSACTIONS ON IMAGE PROCESSING and currently serves as Associate Editor for the IEEE SIGNAL PROCESSING LETTERS. For his research in video tracking, he received an ARO Young Investigator Award. In 1997, he was named the Eta Kappa Nu Outstanding Young Electrical Engineer—a national award that has been given annually since 1936. In 1998, he received the Halliburton Outstanding Young Faculty Award. He is a recipient of the Whitaker Foundation Biomedical Engineering Research Grant.